Simulations of Dissipative, Shore-Oblique Infragravity Waves

STEPHEN M. HENDERSON

College of Oceanic and Atmospheric Sciences, Oregon State University, Corvallis, Oregon

A. J. BOWEN

Department of Oceanography, Dalhousie University, Halifax, Nova Scotia, Canada

(Manuscript received 13 May 2002, in final form 24 October 2002)

ABSTRACT

A model of forced, dissipative shore-oblique shallow water waves predicts net cross-shore infragravity wave propagation, in qualitative agreement with field observations. Forcing applied near the shore generates edge waves, whose energy is mostly trapped shoreward of the edge wave turning point. Forcing applied sufficiently far seaward of the turning point generates only evanescent waves, whose energy decays almost exponentially with distance from regions of forcing. Weakly dissipative edge waves are nearly cross-shore standing, whereas strongly dissipative edge waves propagate obliquely across-shore. Groups of directionally spread incident waves can nonlinearly force evanescent bound waves, which propagate shoreward, lowering the sea level under large incident waves. Unlike the bound waves described by previous researchers, evanescent bound waves are not released when incident waves break and do not radiate far from the breakpoint. Regions of evanescent waves between the shoreface and shore-parallel sandbars are barriers to energy transport, which can decouple bar- and shore-trapped waves even when dissipation is weak.

1. Introduction

Low-frequency (0.005–0.05 Hz) surface gravity waves, called ''infragravity waves'' or ''surf beat,'' can be important inside the surf zone, where they sometimes are more energetic than incident (0.05–0.5 Hz) waves.

Infragravity waves are generated by groups of incident waves. Longuet-Higgins and Stewart (1962) and Hasselmann et al. (1963) predicted that groups of waves propagating over a flat seabed nonlinearly force low frequency ''bound waves.'' These bound waves propagate shoreward, lowering the sea level under groups of large incident waves. Field observations (Hasselmann et al. 1963; Huntley and Kim 1985; Guza et al. 1985; Elgar and Guza 1985a; Ruessink 1998a,b) confirm that the sea level does tend to be lower under groups of large incident waves. In the surf zone, incoming bound waves are in theory modified by intermittent incident-wave breaking (Symonds et al. 1982) before being released as free waves.

Two types of free infragravity wave exist: edge waves and leaky waves. Edge waves are trapped near the shore by refraction, whereas leaky waves can propagate from and to deep water. If dissipation is sufficiently weak, then edge and leaky waves might respond to forcing in a strongly resonant manner and dominate infragravity motions. However, if dissipation is so strong that the parameter

$$Q = 2\pi \frac{\text{total energy of edge or leaky wave mode}}{\text{energy of mode damped in one wave period}} \quad (1)$$

is not much greater than 1, the effects of forcing cannot accumulate over many wave periods and resonance is suppressed (Green 1955; Holman 1981). Bowen and Guza (1978) and others have suggested that resonant edge waves might become larger than leaky waves because they are trapped in shallow water where nonlinear forcing is most effective. Field observations confirm that much infragravity energy does exist in the form of resonant edge waves (Munk et al. 1964; Huntley et al. 1981; Oltman-Shay and Guza 1987). Field observations also show that edge waves can be trapped over offshore sand bars, at both infragravity and incident frequencies (Schönfeldt 1995; Bryan and Bowen 1996; Bryan et al. 1998).

Recent field observations indicate that infragravity waves are only partially reflected from the shore (Nelson and Gonsalves 1992; Saulter et al. 1998; Sheremet et al. 2001, 2002; Henderson et al. 2001; Henderson and Bowen 2002). Apparently, much of the energy carried

Corresponding author address: Dr. Stephen M. Henderson, College of Oceanic and Atmospheric Sciences, Oregon State University, 104 Ocean Admin. Bldg., Corvallis, OR 97331-5503.
E-mail: shenders@coas.oregonstate.edu

by infragravity waves that propagate into the surf zone is somehow lost before the waves can reach the shore, reflect, and propagate back to the edge of the surf zone. Sheremet et al. (2001) found that shoreward-propagating infragravity motions are dominated by waves that approach the shore obliquely, with the frequencies and longshore wavenumbers typical of edge waves. This suggests that the observed shoreward-propagating waves were edge waves, rather than leaky waves. However, cross-shore propagating edge waves are not predicted by classical edge wave models. Instead, classical models (Eckart 1951; Ursell 1952; Ball 1967; Holman and Bowen 1979; Howd et al. 1992; Bryan and Bowen 1996) predict that edge waves are cross-shore standing. This is because classical edge wave models assume that dissipation is very weak.

In an attempt to simulate the progressive infragravity waves observed in the field, Henderson and Bowen (2001) developed a model that includes dissipation at leading order. We describe this model in section 2. The model simulates only shore-oblique shallow water waves and therefore cannot simulate leaky waves. We discuss the possible importance of leaky waves in sections 2 and 3. Section 3 presents model results, including many results not presented by Henderson and Bowen (2001). As expected, strong dissipation introduces cross-shore propagating edge waves. Perhaps more surprising, even weak dissipation ($Q \gg 1$) can strongly modify shore-oblique shallow water waves. In certain cases, including some high Q cases, ''evanescent waves,'' whose energy is trapped near regions of forcing, can dominate over edge waves. Realistic forcing can generate group-bound evanescent waves, which appear very similar to the group-bound waves described by Longuet-Higgins and Stewart (1962) and Hasselmann et al. (1963). However, unlike the bound waves of Longuet-Higgins and Stewart (1962), evanescent bound waves are not released when wave groups are destroyed by breaking. Weak dissipation ($Q \gg 1$) can also have a leading-order effect by decoupling bar- and shore-trapped edge waves. In section 4, we summarize the effects of dissipation on simulated shore-oblique shallow water waves and note several model predictions that could be tested using field data.

2. Model derivation

a. Governing equations

In this section we present a set of equations governing forced, dissipative, shore-oblique shallow water waves.

Let x and y be distance from the shore and distance alongshore, respectively. We will solve for the infragravity sea level displacement η, seaward velocity u, and alongshore velocity v. Groups of incident waves force infragravity waves through infragravity–frequency fluctuations in the the radiation stress $\mathcal{S}$ and in the depth-integrated Stokes drift $\mathbf{M} = (M_x, M_y)$. To simplify the equations of motion, we introduce the ''mass transport velocity'' $\tilde{\mathbf{u}} = (u + M_x/h, v + M_y/h)$, where h is the mean water depth. We neglect the small difference between the still water depth and the mean water depth.

Infragravity waves are modeled using the forced, dissipative shallow-water equations

$$\frac{\partial \tilde{u}}{\partial t} + g\frac{\partial \eta}{\partial x} + \lambda u = -\frac{1}{\rho h}\left(\frac{\partial \mathcal{S}_{xx}}{\partial x} + \frac{\partial \mathcal{S}_{xy}}{\partial y}\right), \quad (2)$$

$$\frac{\partial \tilde{v}}{\partial t} + g\frac{\partial \eta}{\partial y} + \lambda v = -\frac{1}{\rho h}\left(\frac{\partial \mathcal{S}_{yy}}{\partial y} + \frac{\partial \mathcal{S}_{xy}}{\partial x}\right), \quad (3)$$

$$\frac{\partial \eta}{\partial t} + \frac{\partial h\tilde{u}}{\partial x} + \frac{\partial h\tilde{v}}{\partial y} = 0, \quad (4)$$

where

$g \equiv$ gravitational acceleration,

$\rho \equiv$ water density,

and λ is a damping coefficient (here assumed constant). We have assumed that friction acts on the Eulerian flow but not on the Stokes drift.

Let

$$h = \beta x, \quad (5)$$

where β is a constant beach slope.

We have assumed unrealistically simple forms for h and λ. More realistic conditions are simulated by dividing the beach profile into a series of sections, with λ and β constant within each section. Solutions of Eqs. (2)–(5) are calculated for each section and then patched together under the constraint that η and $h\tilde{u}$ are continuous.[1] The matching conditions previously given by Henderson and Bowen (2001) implicitly assume that the right-hand side of Eq. (2) is zero, and therefore they are incorrect.

Assume solutions of the form $\eta = \hat{\eta}(x)e^{i(ky-\omega t)}$, and similarly for u, v, $\mathcal{S}$, and $\mathbf{M}$. The response to arbitrary forcing can be calculated by Fourier superposition. Solving Eqs. (2)–(5) for $\hat{\eta}$ gives

$$\frac{\partial}{\partial x}\left(x\frac{\partial \hat{\eta}}{\partial x}\right) + \left[\frac{\omega^2}{g\beta}\left(1 + i\frac{\lambda}{\omega}\right) - k^2 x\right]\hat{\eta} = \hat{F}, \quad (6)$$

where the dimensionless forcing is

$$\hat{F} = -\frac{1}{\rho g \beta}\left(\frac{\partial^2 \hat{\mathcal{S}}_{xx}}{\partial x^2} + 2ik\frac{\partial \hat{\mathcal{S}}_{xy}}{\partial x} - k^2\hat{\mathcal{S}}_{yy}\right) + \frac{\lambda}{g\beta}\left(\frac{\partial \hat{M}_x}{\partial x} + ik\hat{M}_y\right). \quad (7)$$

[1] According to WKB theory, a sudden change in the bottom slope at $x = x_0$ modifies the shoaling of incident waves so as to add a delta-function forcing at x_0 (Liu 1989). In reality, because of non-WKB effects, this forcing is applied in a small neighborhood of x_0. We simplify the problem by applying the delta function forcing very near, but not exactly at, x_0.

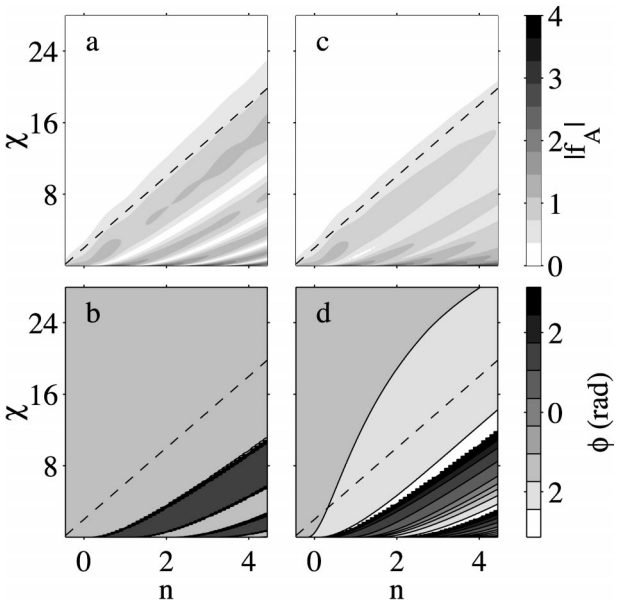

FIG. 1. Dependence of homogeneous solution f_A on mode number n and distance from shore $\chi = 2kx$; dashed line is edge wave turning point: (a), (c) magnitude $|f_A|$ and (b), (d) phase ϕ, where $f_A = |f_A|e^{i\phi}$. In (a) and (b) $\lambda/\omega = 3 \times 10^{-3}$ and in (c) and (d) $\lambda/\omega = 8 \times 10^{-2}$.

If $\lambda = 0$ and $\hat{F} = 0$, then Eq. (6) reduces to the free-edge wave equation (Mei 1983, p. 155).

Equation (6) has a turning point at $x_T = \omega^2/(k^2 g\beta)$, where the longshore phase velocity ω/k equals the shallow-water phase speed $(gh)^{1/2}$. Refraction traps much of the energy of free shallow water waves shoreward of x_T.

Boundary conditions are

$$\lim_{x\to 0} x\frac{\partial \hat{\eta}}{\partial x} = 0, \quad \text{and} \tag{8}$$

$$\hat{\eta} \text{ is bounded as } x \to \infty. \tag{9}$$

b. Solution

Substituting $\chi = 2kx$ and $\tilde{\eta} = e^{kx}\hat{\eta}$ into the homogeneous form of Eq. (6) leads to the confluent hypergeometric equation

$$\chi\frac{\partial^2 \tilde{\eta}}{\partial \chi^2} + (1 - \chi)\frac{\partial \tilde{\eta}}{\partial \chi} + n'\tilde{\eta} = 0, \tag{10}$$

where

$$n' = \frac{1}{2}\left[\frac{\omega^2(1 + i\lambda/\omega)}{kg\beta} - 1\right]. \tag{11}$$

If $n' \notin \{0, 1, 2, 3, \ldots\}$, then two linearly independent homogeneous solutions of Eq. (6) are

$$f_B(kx) = e^{-kx}\,{}_1F_1(-n', 1, 2kx) \quad \text{and} \tag{12}$$

$$f_A(kx) = e^{-kx}U(-n', 1, 2kx), \tag{13}$$

where ${}_1F_1$ and U are confluent hypergeometric functions (Abromowitz and Stegun 1972, sections 13.1.2 and 13.1.6). If $n' \in \{0, 1, 2, 3, \ldots\}$, then f_A is undefined, and f_B reduces to the classical, nondissipative edge wave solution of Eckart (1951). Green (1986) simulated nondissipative edge waves near a seawall using f_A with $\lambda = 0$ and noninteger n'.

We are interested in steady, dissipative waves. For such waves, ω and k are real and $\lambda > 0$, so n' is complex, which implies $n' \notin \{0, 1, 2, 3, \ldots\}$. Now f_B satisfies the shoreline boundary condition [Eq. (8)] but not the seaward boundary condition [Eq. (9)], whereas f_A satisfies the seaward boundary condition but not the shoreline boundary condition. Since no linear combination of f_A and f_B satisfies both boundary conditions, no steady, homogeneous, dissipative solution of Eqs. (6), (8), and (9) exists. This is not surprising since no steady unforced wave field can exist in the presence of dissipation.

We use f_A and f_B to construct forced solutions to Eqs. (6), (8), and (9). The dimensionless Green's function

$$G(x, x_F) = \begin{cases} Bf_B(kx), & x \le x_F \\ Af_A(kx), & x > x_F, \end{cases} \tag{14}$$

where A and B are constants chosen to satisfy

$$\lim_{x\to x_F^+} G(x, x_F) = \lim_{x\to x_F^-} G(x, x_F) \quad \text{and} \tag{15}$$

$$\lim_{x\to x_F^+} \frac{\partial G(x, x_F)}{\partial x} - \lim_{x\to x_F^-} \frac{\partial G(x, x_F)}{\partial x} = \frac{1}{x_F}, \tag{16}$$

is the response at x to point forcing $\hat{F} = \delta(x - x_F)$, where $\delta(x)$ is the Dirac delta function. Therefore, f_A represents waves seaward of the point of forcing, whereas f_B represents waves shoreward of the point of forcing.

The particular solution of Eqs. (6), (8), and (9) for arbitrary $\hat{F}(x)$ is (Arfken and Weber 2001, p. 618)

$$\hat{\eta}(x) = \int_{x_F} G(x, x_F)\hat{F}(x_F)\, dx_F. \tag{17}$$

Therefore, the response to distributed forcing can be viewed as an integral of Green's functions. We describe the cross-shore structure of individual Green's functions in sections 3a–c. Examples of the response to distributed forcing are presented in section 3d.

Here f_A and f_B are functions of the cross-shore distance χ, the dissipation strength λ/ω, and the mode number $n = \Re\{n'\}$. In the absence of forcing and dissipation, edge waves exist on a planar beach for only integer values of n (Eckart 1951). In contrast, forced waves have the wavenumber and frequency of the applied forcing and exist for noninteger values of n. We refer to n as the mode number, even when n takes noninteger values. When n equals (or nearly equals) an integer, energetic, resonant edge waves can be generated [Holman (1981) and references therein].

Figure 1 summarizes the behavior of f_A for n between -0.5 and 4.5. A vertical section through each plot gives

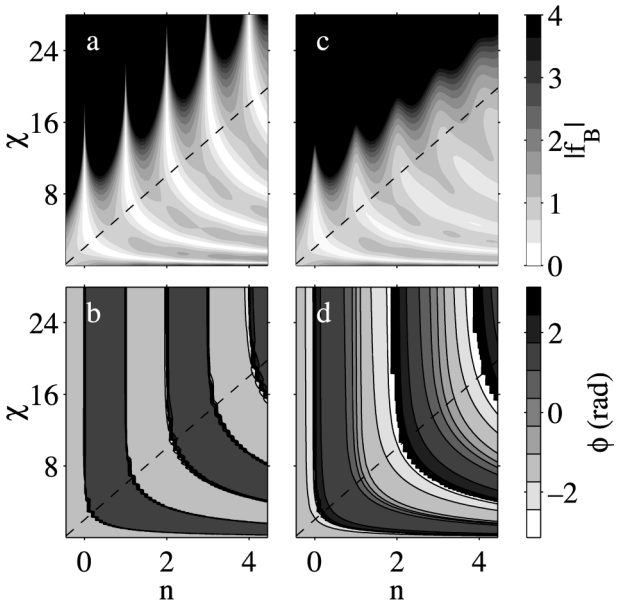

FIG. 2. Dependence of homogeneous solution f_B on mode number n and distance from shore $\chi = 2kx$; dashed line is edge wave turning point: (a), (c) magnitude $|f_B|$ and (b), (d) phase ϕ, where $f_B = |f_B|e^{i\phi}$. In (a) and (b) $\lambda/\omega = 3 \times 10^{-3}$ and in (c) and (d) $\lambda/\omega = 8 \times 10^{-2}$.

the cross-shore structure of the wave field for a particular value of n. Figures 1a,b show weakly dissipative waves, whereas Figs. 1c,d show strongly dissipative waves (f_A has been renormalized so that the mean square magnitude of f_A shoreward of the turning point is equal to 1). Waves propagating seaward, away from regions of forcing, reflect from the turning point, setting up a cross-shore standing wave structure (antinodes appear as dark bands in Fig. 1a; nodes appear as as light bands in Fig. 1a and as $\pm\pi$ phase jumps in Fig. 1b). Outside the turning point, f_A decays almost exponentially. The cross-shore standing structure, clear in the weakly dissipative case (Figs. 1a,b), is modified by dissipation, as shown most clearly in the strongly dissipative case (Figs. 1c,d). Since energy is dissipated as waves propagate to the turning point and back, the nodal structure is incomplete (weakly developed light and dark bands in Fig. 1c) and net seaward propagation results (except for 2π phase wraps, the phase increases smoothly with distance from shore in Fig. 1d).

Figure 2 summarizes the behavior of f_B. Inside the turning point, waves propagate shoreward, away from regions of forcing, and reflect from the shore, setting up a standing wave structure (Figs. 2a,b). Dissipation leads to net shoreward propagation (Fig. 2d) and weakened nodal structure (Fig. 2c). For noninteger mode numbers, f_B grows almost exponentially with distance seaward of the turning point. For near-integer mode numbers, the seaward growth of f_B begins far offshore of the turning point. This growth with distance seaward of the turning point is best viewed as a decay with distance shoreward of regions of forcing. All magnitudes greater than 4 are represented by black shading in Figs. 2a,c. Consequently, much of the region seaward of the turning point, where magnitudes often greatly exceed 4, is black in Figs. 2a,c.

c. Leaky waves

According to our shallow-water model, much of the energy of free shallow water waves is trapped shoreward of a turning point x_T. When the shallow-water assumption is relaxed, free waves are refractively trapped only if $\omega^2 < gk$ (Ursell 1952). If $\omega^2 > gk$, then waves propagate from and to deep water and are called leaky waves. Now $\omega^2/gk = kh_T$, where h_T = depth at x_T. Since our shallow-water model requires $kh_T \ll 1$, leaky waves are excluded from our analysis. We discuss the possible importance of leaky waves in sections 3b and 3d.

3. Model results

In this section we present examples of forced, dissipative shallow water waves. We will show that the cross-shore structure of these dissipative waves depends markedly on the cross-shore structure of the applied forcing.

a. Edge waves

Figure 3 shows Green's functions for dissipative waves of 40-s period forced shoreward of the turning point (x_F = 140 m) on a planar beach of slope 0.02. The cross-shore structure of the weakly dissipated mode-2 wave (Figs. 3a,b) is very similar to the cross-shore structure of a free mode-2 edge wave (Mei 1983, p. 156). The cross-shore structure of the weakly dissipated mode-2.5 wave (Figs. 3c,d) depends on the location of the forcing and differs from the structure of free waves. Figures 3e–h show strongly dissipated mode-2 and mode-2.5 waves. The wave field is now a mixture of cross-shore standing waves and cross-shore propagating waves. Since these waves also propagate alongshore (with speed ω/k), the cross-shore propagating waves of Fig. 3 propagate at an oblique angle to the shore. The mode-2 waves are resonant and consequently have larger amplitudes than the mode-2.5 waves, especially when dissipation is weak. We call all the waves shown in Fig. 3 edge waves because they all are trapped near the edge of the ocean by refraction.

b. Evanescent waves

Forcing applied shoreward of the edge wave turning point generates edge waves (section 3a). Figure 4 shows that very different behavior can result when forcing is applied seaward of the turning point (x_F = 100 m, $x_T \approx 8$ m). Only when forcing was resonant, and dissipation was extremely weak, were energetic edge waves

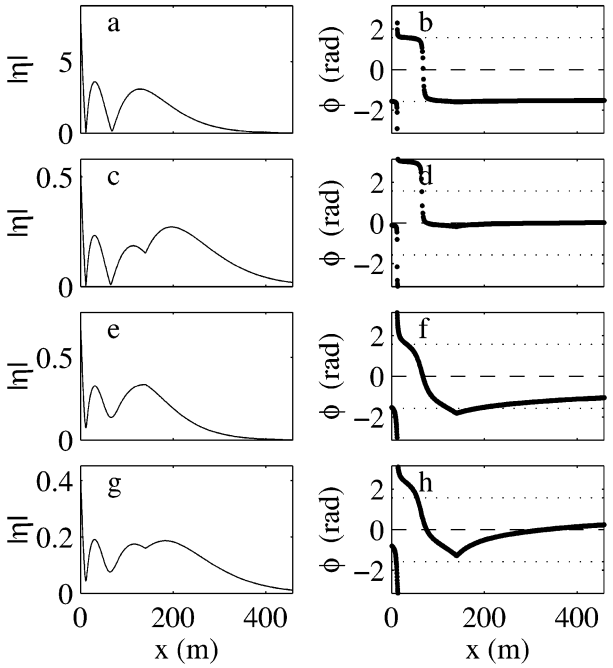

FIG. 3. Point-forced edge wave (a), (c), (e), (g) magnitude $|\eta|$ and (b), (d), (f), (h) phase ϕ: (a), (b) resonant ($n = 2$), weak dissipation ($\lambda/\omega = 1.6 \times 10^{-2}$; (c), (d) nonresonant ($n = 2.5$), weak dissipation ($\lambda/\omega = 1.6 \times 10^{-2}$); (e), (f) resonant ($n = 2$), strong dissipation ($\lambda/\omega = 1.6 \times 10^{-1}$); and (g), (h) nonresonant ($n = 2.5$), strong dissipation ($\lambda/\omega = 1.6 \times 10^{-1}$).

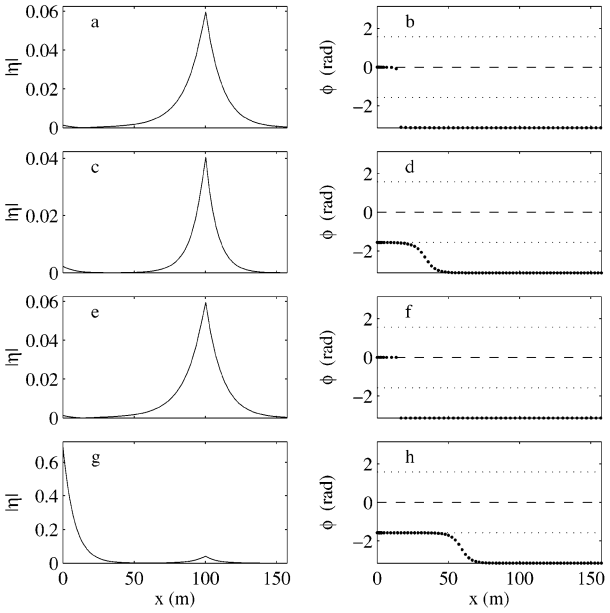

FIG. 4. Point-forced evanescent and edge waves with wave period 40 s, showing (a), (c), (e), (g) magnitude $|\eta|$ and (b), (d), (f), (h) phase ϕ: (a), (b) nonresonant ($n = 0.2$), weak dissipation ($\lambda/\omega = 3 \times 10^{-3}$); (c), (d) resonant ($n = 0$), weak dissipation ($\lambda/\omega = 3 \times 10^{-3}$); (e), (f) nonresonant ($n = 0.2$), very weak dissipation ($\lambda/\omega = 1 \times 10^{-5}$); and (g), (h) resonant ($n = 0$), very weak dissipation ($\lambda/\omega = 1 \times 10^{-5}$).

excited (Figs. 4g,h). Otherwise, only localized waves were generated (Figs. 4a–f). These waves were evanescent; that is, they did not propagate freely but decayed approximately exponentially with distance away from the point of forcing.

A simple model explains the behavior shown in Fig. 4. Since forcing is applied only outside the turning point, the mean energy flux carried to the turning point by evanescent waves q_T must balance the mean edge wave dissipation rate $\mathcal{D}$. We estimate the relative amplitudes of edge and evanescent waves by equating approximate expressions for q_T and $\mathcal{D}$.

From Eq. (1)

$$\mathcal{D} = \frac{\omega g a_{\text{edge}}^2 x_T}{Q}, \tag{18}$$

where $g a_{\text{edge}}^2 x_T$ is the total energy of the edge wave, and a_{edge} is a typical edge wave amplitude.

A crude approximation of the cross-shore structure of evanescent waves is

$$\hat{\eta} \approx a_1 e^{-K(x - x_T)} + a_2 e^{i\phi} e^{K(x - x_F)}, \tag{19}$$

where a_1 and a_2 are approximately the evanescent wave magnitudes at x_T and x_F, respectively, and ϕ is a real constant. The cross-shore e-folding distance for evanescent waves is

$$K^{-1} \approx [k^2 - \omega^2/(g h_{1/2})]^{-1/2}, \tag{20}$$

where $h_{1/2} = \beta(x_T + x_F)/2$ is the depth half way between the point of forcing and the turning point. The energy flux q_T carried by evanescent waves is mathematically analogous to the probability flux carried by quantum-mechanical particles tunneling through a potential barrier (Ohanian 1990, section 3), and equals the mean depth-integrated product of pressure and velocity. From Eqs. (2) and (19),

$$q_T \approx \frac{2Khg^2}{\omega} e^{-KL} a_1 a_2 \sin(\phi), \tag{21}$$

where $L = x_F - x_T$. When KL is large, evanescent waves decay greatly between the point of forcing and the turning point, and they carry very little energy to the turning point.

Equating q_T with $\mathcal{D}$ and noting that $h/x_T \approx \beta$, $a_1 \approx a_{\text{edge}}$, $a_2 \approx a_{\text{ev}}$ (where a_{ev} is the evanescent wave amplitude at x_F), leads to

$$\frac{a_{\text{edge}}}{a_{\text{ev}}} \approx \frac{K \sin(\phi)}{k(n + 1/2)} Q e^{-KL}. \tag{22}$$

The ratio between edge and evanescent wave amplitudes depends on their relative phase ϕ. For resonant edge waves, $\phi \approx \pi/2$, and so $\sin(\phi) \approx 1$ (e.g., Figs. 4d,h). In contrast, ϕ can be close to π or 0 [and so $\sin(\phi)$ can be much less than 1] if edge waves are nonresonant (e.g., Figs. 4b,f). Figure 5 shows that Eq. (22), with $\sin(\phi) = 1$, predicted the ratio between evanescent and resonant edge wave amplitudes to within a factor of 2,

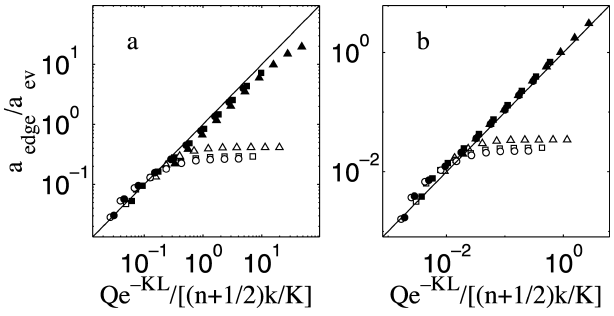

FIG. 5. Ratio between edge and evanescent wave amplitudes, a_{edge}/a_{ev}, vs ratio predicted by Eq. (22), with $\sin(\phi) = 1$, wave period 40 s, and $\beta = 0.02$: (a) $KL = 2$ and (b) $KL = 5$. Solid black symbols indicate resonant waves: $n = 0, 1, 2$ for triangles, squares, and circles, respectively. Open symbols indicate nonresonant waves: $n = 0.25$, 1.25, 2.25 for triangles, squares, and circles, respectively.

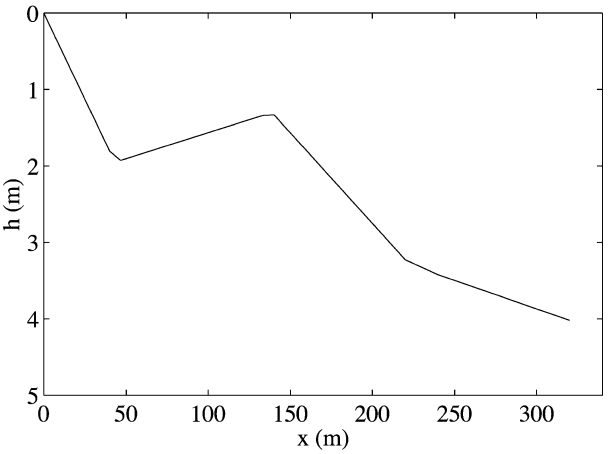

FIG. 6. Barred beach profile. Water depth h vs distance from shore x. Beach slope is constant seaward of $x = 220$ m.

except when edge waves were much larger than evanescent waves ($a_{edge}/a_{ev} \approx 10$) and KL was small [Eq. (22) was inaccurate when $KL < 2$]. Nonresonant edge waves are much smaller than evanescent waves when KL is sufficiently large. If forcing is broadbanded, then the bandwidth of the spectral peaks associated with resonant edge waves is $O(Q^{-1})$, and so the ratio between total edge and evanescent wave energy scales with $Qe^{-2KL}/[(n + 1/2)k/K]^2$. When KL is large, evanescent waves can dominate over edge waves, even if Q is much greater than 1.

In a classic paper, Munk et al. (1964) commented that they "... failed to generate observable edge waves by racing a destroyer at 31 knots along the 20-fathom line from La Jolla to Oceanside." The destroyer traveled outside the turning point of shallow water waves, a fact that might explain the failure to generate edge waves (although departures from shallow-water theory, together with uncertainty about the strength of dissipation, make it difficult to draw strong conclusions). To ensure that forcing was applied inside the turning point, a boat would have to travel faster, or in shallower water.

When $\omega^2 > gk$, the shallow-water approximation fails, and waves are leaky. Leaky waves are never evanescent and consequently always can radiate far from regions of forcing.

c. Dissipative decoupling

Schönfeldt (1995), Bryan and Bowen (1996), and Bryan et al. (1998) showed that refraction can trap edge waves over sandbars. When waves are trapped over sandbars, evanescent waves exist between the sandbar and the beach. Evanescent waves transport very little energy over cross-shore distances large compared with $(k^2 - \omega^2/gh)^{-1/2}$ (section 3b). Consequently, the region of evanescent waves shoreward of the sandbar is a barrier to energy transport, which can effectively decouple dissipative bar- and shore-trapped waves.

If forcing is applied only over the sandbar and evanescent waves exist between the sandbar and the shore, then an argument similar to the one used to derive Eq. (22) leads to

$$\frac{a_{shore}}{a_{bar}} \approx \frac{K \sin(\phi)}{k(n + 1/2)} Qe^{-KL}, \tag{23}$$

where a_{shore} and a_{bar} are the amplitudes of shore- and bar-trapped waves respectively, L is the width of the region of evanescent waves in the trough, ϕ is the phase between bar- and shore-trapped waves at their turning points, and n is the mode number of the shore-trapped wave. Here K^{-1} is the e-folding distance for evanescent waves in the trough, which we crudely approximate by $[k^2 - 2\omega^2/g(h_T + h_{trough})]^{-1/2}$, where h_T is the turning depth and h_{trough} is the maximum water depth shoreward of the bar. As in section 3b, $\sin(\phi)$ is about 1 (zero) if shore-trapped waves are (are not) resonant.

If forcing is applied over the shoreface, but not over the bar, then a_{bar}/a_{shore} approximately equals the negative of the right-hand side of Eq. (23) (the term $n + 1/2$ is modified, but on realistic beaches the order of magnitude of a_{bar}/a_{shore} remains unchanged).

If $Qe^{-KL}/[(n + 1/2)k/K] \ll 1$, then forcing over the bar does not generate significant shore-trapped waves, and forcing over the shoreface does not generate significant bar-trapped waves.

An example of a barred beach is shown in Fig. 6. We solve Eqs. (2), (3), and (4) for the beach shown in Fig. 6 by patching together planar beach solutions. Figure 7a shows how the total potential energy of weakly dissipative waves, $V = g\int_{x=0}^{\infty} |\hat{\eta}(x)|^2 \, dx/2$, depends on the cyclic frequency ω_c and cyclic wavenumber k_c of unit forcing applied 0.3 m from the shore [$\hat{F} = \delta(x - 0.3\text{m})$, $\omega_c = \omega/(2\pi)$, $k_c = k/(2\pi)$]. Here V was not calculated in the region $\omega^2 > gk/3$, where shallow-water theory is inaccurate (section 2c).

Shoreward of the trough, the barred beach of Fig. 6 has a slope of 0.045. Consequently, resonant waves

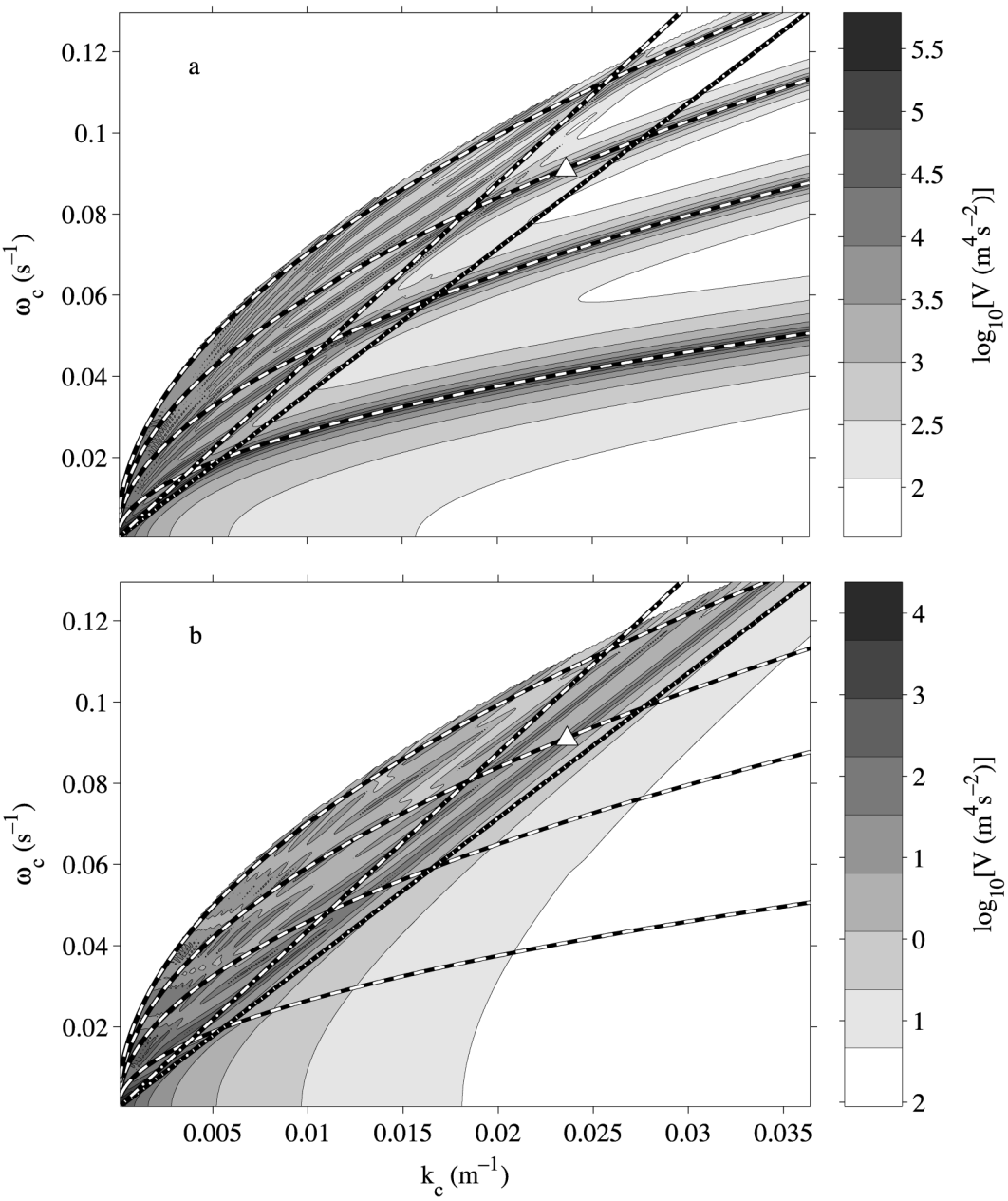

FIG. 7. Potential energy V of weakly dissipative ($\lambda = 5 \times 10^{-3}$ s^{-1}) waves vs cyclic frequency ω_c and longshore cyclic wavenumber k_c for (a) forcing applied near the shore and (b) forcing applied over the sandbar. Dashed black and white lines indicate resonances on a planar beach of slope 0.045. Dotted and dash–dotted white lines on black background indicate $\omega/k = (gh_{\text{bar}})^{1/2}$ and $\omega/k = (gh_{\text{trough}})^{1/2}$, respectively. Triangles mark $(\omega_c, k_c) = (0.090\ 96\ \text{s}^{-1}, 0.0236\ \text{m}^{-1})$.

trapped shoreward of the trough have wavenumbers and frequencies near the wavenumbers and frequencies of resonant edge waves on a planar beach of slope 0.045. Resonance curves for bar-trapped waves are lines lying slightly above and almost parallel to $\omega/k = (gh_{\text{bar}})^{1/2}$, where h_{bar} is the depth over the bar crest (Bryan and Bowen 1996).

Forcing applied over the shoreface excited resonant shore-trapped waves, and much energy was concentrated along planar-beach resonance curves (Fig. 7a). At incident frequencies, dissipation decoupled shore- and bar-trapped waves, and so energy was not concentrated along bar-trapped resonance curves. At low infragravity frequencies (<0.02 Hz), resonant waves have wavelengths comparable to the distance from the shore to the bar, and so shore- and bar-trapped waves are not fully decoupled [KL is small; see Eq. (23)]. Energy is concentrated along a line near $\omega/k = (gh_{\text{bar}})^{1/2}$ at low in-

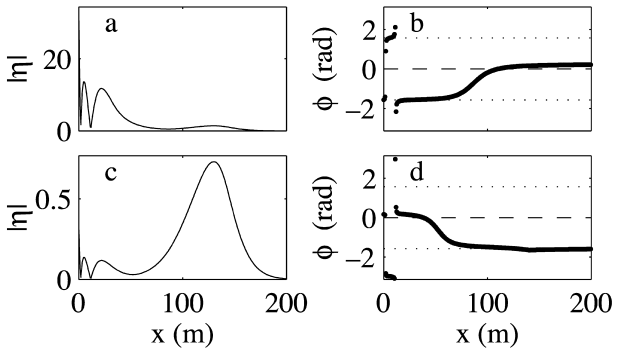

FIG. 8. Weakly dissipative ($\lambda = 5 \times 10^{-3}$ s^{-1}) waves of cyclic frequency 0.090 96 Hz and cyclic wavenumber 0.0236 m^{-1}: (a), (c) magnitude $|\eta|$ and (b), (d) phase ϕ for (a), (b) forcing near shore and (c), (d) forcing near bar crest.

fragravity frequencies, indicating that the bar did influence these waves. Waves with longshore phase velocities greater than $(gh_{\text{trough}})^{1/2}$ propagate freely between the shoreface and the bar (Bryan and Bowen 1996, case 4, p. 6546). Consequently, the resonance curves associated with these waves are influenced by the presence of the bar, and differ from the planar beach resonance curves.

Forcing applied over the bar ($x_F = 140$ m) generated resonant bar-trapped waves. Consequently, much energy was concentrated along resonance lines lying just above $\omega/k = (gh_{\text{bar}})^{1/2}$ (Fig. 7b). Dissipation has decoupled bar- and shore-trapped motions, and so forcing over the bar has not excited waves trapped shoreward of the trough.

Comparison of Figs. 7a and 7b shows that the number of resonance curves, and their location in (ω, k) space, can depend on the location of the forcing, even when Q is much greater than 1 [here $Q \approx 60$ for $(\omega_c, k_c) = (0.09$ Hz, 0.024 m$^{-1})$].

Let $\omega_r = 0.090\ 96$ Hz and $k_r = 0.0236$ m^{-1}. At (ω_r, k_r) (marked with triangles in Fig. 7), resonance curves for bar-trapped and shore-trapped motions cross, and the cross-shore structure of dissipative waves depends entirely on where they are forced (Fig. 8). The shore-forced wave is a resonant mode-2 shore-trapped wave (Figs. 8a,b). The bar-forced wave is a resonant mode-0 bar-trapped wave (Figs. 8c,d). Equation (23) predicts $a_{\text{shore}}/a_{\text{bar}} = 0.13$ when forcing is applied over the bar, roughly consistent with Fig. 8c.

Nondissipative theories predict that the region near (ω_r, k_r) is a mode coupling region, within which two resonance curves pass very close together but do not cross [this is the ''kissing mode'' case described by Bryan and Bowen (1996). Discussions of mode coupling in other physical contexts are given by Eckart (1961), Parrish and Niiler (1971), Louisell (1960), and Flynn and Littlejohn (1994)]. Because dissipation has decoupled bar- and shore-trapped waves, no sign of such separated resonance curves can be seen in Fig. 7. We obtained two separate resonance curves near (ω_r, k_r) from the dissipative model only when dissipation was unrealistically weak ($Q > 10^3$, not shown). The fact that dissipation can overwhelm weak mode coupling was previously noted in the context of atmospheric edge waves by Garrett (1969).

d. Distributed forcing and variable dissipation

This section presents simulations of waves generated by distributed forcing in the presence of spatially varying dissipation. These simulations show that, given realistic forcing and dissipation, both edge and evanescent waves propagate obliquely shoreward into the outer surf zone, in qualitative agreement with field observations. For all simulations presented in this section, the beach profile is the one shown in Fig. 6.

A standard bottom friction parameterization suggests

$$\lambda = C|\mathbf{u}|h, \tag{24}$$

where $|\mathbf{u}|$ is a typical water speed and C is a constant. For steady currents in the surf zone, $C \approx 3 \times 10^{-3}$ (Feddersen et al. 1998), whereas for waves on the continental shelf with periods of about 10 s, $C \approx 5 \times 10^{-2}$ (Herbers et al. 2000). We do not know what value C should take for infragravity waves. We assume $C = 10^{-2}$. To simulate dissipation when incident waves were small (large), we assume $|\mathbf{u}| = 0.3$ m s^{-1} ($|\mathbf{u}| = 1$ m s^{-1}). Equation (24) fails as h tends to zero [in the absence of capillary forces, Eq. (24) predicts total absorption (zero reflection) of linear waves at the shore (Miles 1990)]. To avoid this problem, we arbitrarily set all values of λ shoreward of $h = 0.5$ m equal to $C|\mathbf{u}|/(0.5$ m). We divided the region seaward of $h = 0.5$ m into a series of segments, each 10 m wide, and calculated one value of λ for each segment by substituting the local mean depth into Eq. (24).

Infragravity waves are forced by groups of higher-frequency waves. We assume that wave groups, with cyclic frequency ω and cyclic longshore wavenumber k, are produced by interference between two sinusoidal wave trains with frequencies ω_s and $\omega_s + \omega$, and longshore wavenumbers k_s and $k_s + k$. We consider only two group frequencies ($\omega = 0.023$ and 0.037 Hz). We assume $k = 0.005$ m^{-1}, $\omega_s = 0.01$ Hz, and $k_s = -k/2$. We calculate the complex amplitudes, a_{s1} and a_{s2}, of sea level fluctuations produced by the two wave trains by assuming linear, nondissipative, Wentzel–Kramers–Brillouin (WKB) shoaling of shoreward-propagating waves over an alongshore-uniform beach [giving Eq. (2) of Guza and Bowen (1977), with $r = 0$, for each velocity potential]. This approach neglects both nonlinear generation of harmonics (Freilich and Guza 1984; Elgar and Guza 1985a,b) and the increase in directional spread that accompanies wave breaking (Herbers et al. 1999). The complex amplitude of fluctuations in the energy of nondissipative incident waves is $a_G^{(1)} = g a_{s1} a_{s2}^*$. Wave groups are partially destroyed in the outer surf zone by wave breaking (Symonds et al. 1982; List

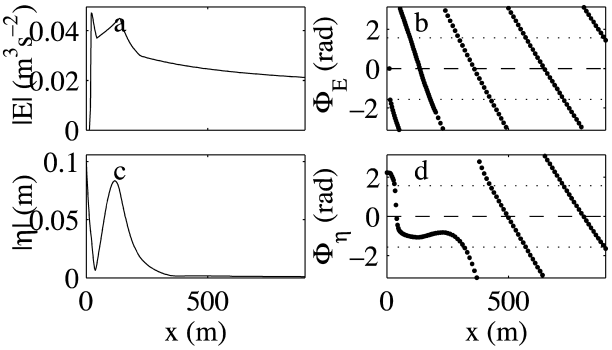

FIG. 9. Low-frequency (0.023 Hz) groups of (a), (b) small incident waves and (c), (d) associated infragravity waves: (a), (c) magnitude and (b), (d) phase.

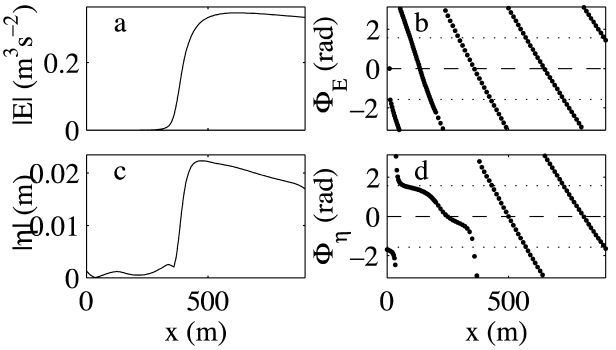

FIG. 11. As in Fig. 9 but for low-frequency (0.023 Hz) groups of (a), (b) large incident waves and (c), (d) associated infragravity waves.

1991; Haller and Dalrymple 1995). We simulate breaking by assuming

$$a_G(x) = \frac{1 + \tanh[\zeta(x - x_b)]}{2} a_G^{(1)}(x), \qquad (25)$$

where $a_G(x)$ is the amplitude of group-frequency energy fluctuations in the presence of breaking. The constants x_b and ζ determine, respectively, the location of the outer edge of the surf zone and the width of the region over which wave groups are destroyed. We substituted a_G into energy-based formulas for the Stokes drift and radiation stress (Whitham 1962) and then calculated the nonlinear forcing $\hat{F}$ from Eq. (7).

When incident waves were small, groups propagated into very shallow water, and so even those edge waves that were trapped very close to the shore were excited. Figure 9 shows that relatively low frequency (0.023 Hz) groups of small incident waves generated a resonant, cross-shore standing, mode-1 edge wave. Higher-frequency (0.037 Hz) groups generated a resonant, cross-shore standing, mode-5 edge wave (Fig. 10).

When incident waves were large, breaking destroyed wave groups far offshore. Consequently, although relatively low frequency (0.023 Hz) groups resonated with a mode-1 edge wave, no significant edge wave was generated (Fig. 11). Instead, only evanescent waves were generated. These evanescent waves propagated shoreward with the short-wave groups, lowering the sea level under large incident waves (Figs. 11b,d). In this regard, these waves were similar to the bound waves described by Longuet-Higgins and Stewart (1962). However, the bound waves considered here are evanescent, and so they do not radiate far from regions of forcing (section 3b). In contrast, the waves considered by Longuet-Higgins and Stewart (1962) are not evanescent (this is ensured by their assumption that forcing is unidirectional) and do radiate far from regions of forcing. Consequently, whereas the bound waves of Longuet-Higgins and Stewart (1962) might be released when short waves break, evanescent bound waves are not released and do not radiate away from the breakpoint.

Higher-frequency (0.037 Hz; Fig. 12) forcing resonates with a higher-mode-number ($n = 5$) edge wave, whose turning point is seaward of the breakpoint. Now energetic edge waves are generated and propagate shoreward. Strong dissipation in shallow water [Eq. (24)], combined with a lack of forcing inside the surf zone, ensures that these edge waves propagate shoreward (rather than seaward) near the edge of the surf zone, consistent with field observations. Outside the turning point, shoreward-propagating evanescent bound waves can still be seen.

Forcing with a frequency greater than $(gk)^{1/2}$ generates

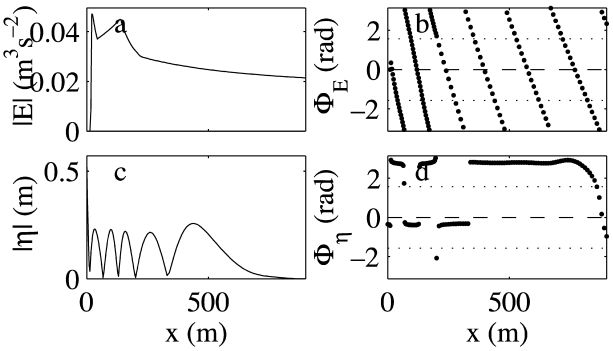

FIG. 10. As in Fig. 9 but for high-frequency (0.037 Hz) groups of (a), (b) small incident waves and (c), (d) associated infragravity waves.

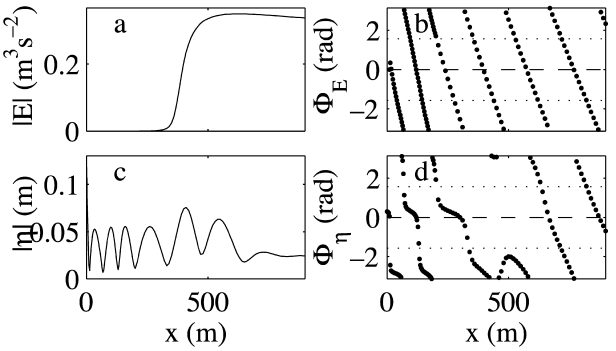

FIG. 12. As in Fig. 9 but for high-frequency (0.037 Hz) groups of (a), (b) large incident waves and (c), (d) associated infragravity waves.

leaky waves. Leaky waves are never evanescent and, when forced, always radiate away from the breakpoint.

We have introduced two types of cross-shore propagating infragravity waves: dissipative edge waves and evanescent bound waves. Since evanescent waves exist only seaward of a turning point, we can be sure that edge waves are more energetic than evanescent waves at the shore. Unfortunately, we cannot use our model to predict which type of wave is most energetic farther offshore because both forcing and dissipation are poorly understood. The infragravity wave drag coefficient C could take any value between 3×10^{-3} (a typical value for mean currents) and 5×10^{-2} (a typical value for incident waves). The standard drag parameterization [Eq. (24)] is singular at the shore, and the manner in which this singularity is removed has a major effect on the wave field. The strength of surf beat forcing inside the surf zone is not known, but such forcing might play an important role by exciting edge waves that are trapped inside the surf zone. In the next section, we discuss how field data might be used to determine the relative importance of edge waves and evanescent bound waves.

4. Discussion and conclusions

A model of dissipative, shore-oblique shallow water waves suggests that the shoreward-propagating infragravity waves observed in the field could be dissipative edge waves or evanescent bound waves. When dissipation is weak, forcing close to the shore generates cross-shore standing edge waves. Stronger dissipation introduces edge waves that progress obliquely alongshore. Evanescent waves, which decay almost exponentially with distance from regions of forcing, dominate over resonant edge waves when forcing is applied sufficiently far outside the edge-wave turning point. Group-bound evanescent waves propagate shoreward with short-wave groups, lowering the sea level under large incident waves. However, unlike the group-bound waves described by previous researchers, evanescent bound waves are not released when short waves break.

Model results suggest that dissipation might decouple bar- and shore-trapped waves so that forcing over the bar generates only bar-trapped waves and forcing over the shoreface generates only shore-trapped waves. Decoupling is most effective when the wave frequency is high and the trough between the shore and the bar is wide and deep.

Given the current lack of understanding of both incident wave breaking and infragravity wave dissipation, field observations will be required to determine whether the phenomena described above are important on natural beaches.

For shallow-water evanescent waves, $\omega/k < (gh)^{1/2}$. Consequently, it might be possible to estimate evanescent wave energy from band-integrated wavenumber–frequency spectra [Howd et al. (1991) and Noyes et al. (2002) used a similar approach to estimate shear wave energy]. Evanescent waves are most likely to be found in the outer surf zone, especially when the height and directional spread of incident waves are both large.

On natural beaches, during storms, infragravity energy levels do not decay seaward at the rate predicted by free wave theories (Ruessink 1998b; Lippmann et al. 1998, 2001). This might be explained by preferential forcing of partially decoupled bar-trapped waves or by decay of shoreward-propagating edge waves or evanescent bound waves in the outer surf zone. Further observations will be required to test these suggestions.

Acknowledgments. This research was supported by the Andrew Mellon Foundation, the Izaak Walton Killam Foundation, and the Natural Sciences and Engineering Research Council of Canada.

REFERENCES

Abromowitz, M., and L. Stegun, Eds., 1972: *Handbook of Mathematical Functions.* 10th ed. U.S. Department of Commerce, 1046 pp.

Arfken, G. B., and H. J. Weber, 2001: *Mathematical Methods for Physicists.* 5th ed. Academic Press, 1112 pp.

Ball, F., 1967: Edge waves in an ocean of finite depth. *Deep-Sea Res.,* **14,** 79–88.

Bowen, A., and R. Guza, 1978: Edge waves and surf beat. *J. Geophys. Res.,* **83,** 1913–1920.

Bryan, K., and A. Bowen, 1996: Edge wave trapping and amplification on barred beaches. *J. Geophys. Res.,* **101,** 6543–6552.

——, P. Howd, and A. Bowen, 1998: Field observations of bar-trapped edge waves. *J. Geophys. Res.,* **103,** 1285–1305.

Eckart, C., 1951: Surface waves in water of variable depth. Wave Rep. 100, Scripps Institution of Oceanography, La Jolla, CA, 99 pp.

——, 1961: Internal waves in the ocean. *Phys. Fluids,* **4,** 791–799.

Elgar, S., and R. Guza, 1985a: Observations of bispectra of shoaling surface gravity waves. *J. Fluid Mech.,* **161,** 425–448.

——, and ——, 1985b: Shoaling gravity waves: Comparisons between field observations, linear theory, and a nonlinear model. *J. Fluid Mech.,* **158,** 47–70.

Feddersen, F., R. Guza, S. Elgar, and T. Herbers, 1998: Alongshore momentum balances in the nearshore. *J. Geophys. Res.,* **103,** 15 667–15 676.

Flynn, W. G., and R. G. Littlejohn, 1994: Normal forms for linear mode conversion and Landau–Zerner transitions in one dimension. *Ann. Phys.,* **234,** 334–403.

Freilich, M., and R. Guza, 1984: Nonlinear effects on shoaling surface gravity waves. *Philos. Trans. Roy. Soc. London,* **311,** 1–41.

Garrett, C., 1969: Atmospheric edge waves. *Quart. J. Roy. Meteor. Soc.,* **95,** 731–753.

Green, E. I., 1955: The story of *Q. Amer. Sci.,* **43,** 584–594.

Green, T., 1986: Edge waves near a seawall. *Coastal Eng.,* **10,** 119–125.

Guza, R., and A. Bowen, 1977: Resonant interactions for waves breaking on a beach. *Proc. 15th Int. Conf. on Coastal Engineering,* Honolulu, HI, ASCE, 560–579.

——, E. Thornton, and R. Holman, 1985: Swash on steep and shallow beaches. *Proc. 19th Int. Conf. on Coastal Engineering,* Houston, TX, ASCE, 708–723.

Haller, M. C., and R. A. Dalrymple, 1995: Looking for wave groups in the surf zone. *Coastal Dynamics '95,* W. R. Dally and R. B. Zeidler, Eds., ASCE, 81–92.

Hasselmann, K., W. Munk, and G. MacDonald, 1963: Bispectra of

ocean waves. *Proceedings of the Symposium on Time Series Analysis*, M. Rosenblatt, Ed., John Wiley and Sons, 125–139.
Henderson, S. M., and A. Bowen, 2001: The dynamics of dissipative edge waves. *Coastal Dynamics '01*, H. Hanson and M. Larson, Eds., ASCE, 263–271.
——, and ——, 2002: Observations of surf beat forcing and dissipation. *J. Geophys. Res.*, **107,** 3193, doi:10.1029/2000JC000498.
——, S. Elgar, and A. Bowen, 2001: Observations of surf beat propagation and energetics. *Proc. 27th Int. Conf. on Coastal Engineering*, Sydney, Australia, ASCE, 1412–1421.
Herbers, T., S. Elgar, and R. Guza, 1999: Directional spreading of waves in the nearshore. *J. Geophys. Res.*, **104,** 7683–7693.
——, E. Hendrickson, and W. O'Rielly, 2000: Propagation of swell across a wide continental shelf. *J. Geophys. Res.*, **105,** 19 729–19 737.
Holman, R., 1981: Infragravity energy in the surf zone. *J. Geophys. Res.*, **86,** 6442–6450.
——, and A. Bowen, 1979: Edge waves on complex beach profiles. *J. Geophys. Res.*, **84,** 6339–6346.
Howd, P., J. Oltman-Shay, and R. Holman, 1991: Wave variance partitioning in the trough of a barred beach. *J. Geophys. Res.*, **96,** 12 781–12 795.
——, A. Bowen, and R. A. Holman, 1992: Edge waves in the presence of strong longshore currents. *J. Geophys. Res.*, **97,** 11 357–11 371.
Huntley, D. A., and C. S. Kim, 1985: Is surf beat forced or free? *Proc. 19th Int. Conf. on Coastal Engineering*, Houston, TX, ASCE, 871–885.
——, R. Guza, and E. Thornton, 1981: Field observations of surf beat. 1. Progressive edge waves. *J. Geophys. Res.*, **86,** 6451–6466.
Lippmann, T., T. Herbers, and E. Thornton, 1998: Cross-shore variability of infragravity wave pressure and velocities on a barred beach. *Coastal Dynamics '97*, E. B. Thornton, Ed., ASCE, 1023–1032.
——, ——, and ——, 2001: Observations of infragravity waves in the nearshore. *Coastal Dynamics '01*, H. Hanson and M. Larson, Eds., ASCE, 55–61.
List, J. H., 1991: Wave groupiness variations in the nearshore. *Coastal Eng.*, **15,** 475–496.
Liu, P. L., 1989: A note on long waves induced by short-wave groups over a shelf. *J. Fluid Mech.*, **205,** 163–170.
Longuet-Higgins, M., and R. Stewart, 1962: Radiation stress and mass transport in gravity waves, with application to 'surf beats.' *J. Fluid Mech.*, **13,** 481–504.
Louisell, W. H., 1960: *Coupled Mode and Parametric Electronics*. John Wiley and Sons, 268 pp.
Mei, C. C., 1983: *The Applied Dynamics of Ocean Surface Waves*. John Wiley and Sons, 740 pp.
Miles, J., 1990: Wave reflection from a gently sloping beach. *J. Fluid Mech.*, **214,** 59–66.
Munk, W., F. Snodgrass, and F. Gilbert, 1964: Long waves on the continental shelf: An experiment to separate leaky and trapped waves. *J. Fluid Mech.*, **20,** 529–554.
Nelson, R., and J. Gonsalves, 1992: Surf zone transformation of wave height to water depth ratios. *Coastal Eng.*, **17,** 49–70.
Noyes, T. J., R. Guza, S. Elgar, and T. Herbers, 2002: Comparison of methods for estimating nearshore shear wave variance. *J. Atmos. Oceanic Technol.*, **19,** 136–143.
Ohanian, H. C., 1990: *Principles of Quantum Mechanics*. Prentice Hall, 417 pp.
Oltman-Shay, J., and R. Guza, 1987: Infragravity edge wave observations on two California beaches. *J. Phys. Oceanogr.*, **17,** 644–663.
Parrish, D. F., and P. P. Niiler, 1971: Topographic generation of long internal waves in a channel. *Geophys. Fluid Dyn.*, **2,** 1–15.
Ruessink, B., 1998a: Bound and free infragravity waves in the nearshore zone under breaking and non-breaking conditions. *J. Geophys. Res.*, **103,** 12 795–12 805.
——, 1998b: The temporal and spatial variability of infragravity energy in a barred nearshore zone. *Cont. Shelf Res.*, **18,** 585–605.
Saulter, A. N., T. J. O'Hare, and P. E. Russell, 1998: Analysis of infragravity wave-driven sediment transport on macrotidal beaches. *Coastal Dynamics '97*, E. B. Thornton, Ed., ASCE, 1033–1042.
Schönfeldt, H.-J., 1995: On the modification of edge waves by longshore currents. *Cont. Shelf Res.*, **15,** 1213–1220.
Sheremet, A., R. Guza, S. Elgar, and T. Herbers, 2001: Estimating infragravity wave properties from pressure-current meter array observations. *Proc. 27th Inter. Conf. on Coastal Engineering*, Sydney, Australia, ASCE, 1476–1489.
——, ——, ——, and ——, 2002: Observations of nearshore infragravity waves: Seaward and shoreward propagating components. *J. Geophys. Res.*, **107,** 3095, doi:10.1029/2001JC000970.
Symonds, G., D. Huntley, and A. Bowen, 1982: Two-dimensional surf beat: Long wave generation by a time-varying breakpoint. *J. Geophys. Res.*, **87,** 492–498.
Ursell, F., 1952: Edge waves on a sloping beach. *Proc. Roy. Soc. London*, **214A,** 79–97.
Whitham, G., 1962: Mass, momentum and energy flux in water waves. *J. Fluid Mech.*, **12,** 135–147.